# XPO1 inhibition synergizes with PARP1 inhibition in small cell lung cancer by targeting nuclear transport of FOXO3a

Jingya Wang [a,b,c,d], Tao Sun [e,f], Zhaoting Meng [a,b,c,d], Liuchun Wang [a,b,c,d], Mengjie Li [a,b,c,d], Jinliang Chen [a,b,c,d], Tingting Qin [a,b,c,d], Jiangyong Yu [g,h], Miao Zhang [i], Zhixin Bie [j], Zhiqiang Dong [e], Xiangli Jiang [a,b,c,d], Li Lin [a,b,c,d], Cuicui Zhang [a,b,c,d], Zhujun Liu [a,b,c,d], Richeng Jiang [a,b,c,d], Guang Yang [e,****], Lin Li [g,h,***], Yan Zhang [i,**], Dingzhi Huang [a,b,c,d,*]

[a] Tianjin Medical University Cancer Institute & Hospital, National Clinical Research Center for Cancer, PR China
[b] Key Laboratory of Cancer Prevention and Therapy, Tianjin, PR China
[c] Tianjin's Clinical Research Center for Cancer, PR China
[d] Department of Thoracic Oncology, Tianjin Lung Cancer Center, Tianjin Cancer Institute & Hospital, Tianjin Medical University, Tianjin, 300060, PR China
[e] State Key Laboratory of Medicinal Chemical Biology and College of Pharmacy, Nankai University, Tianjin, PR China
[f] Tianjin Key Laboratory of Molecular Drug Research, Tianjin International Joint Academy of Biomedicine, Tianjin, PR China
[g] Department of Medical Oncology, Beijing Hospital, National Center of Gerontology, PR China
[h] Institute of Geriatric Medicine, Chinese Academy of Medical Sciences, PR China
[i] Department of Oncology, The No.1 Hospital of Shijiazhuang, Shijiazhuang, Hebei, 050010, PR China
[j] Minimally Invasive Tumor Therapies Center, Beijing Hospital, National Center of Gerontology, Institute of Geriatric Medicine, Chinese Academy of Medical Sciences, PR China

## ARTICLE INFO

## ABSTRACT

Patient mortality rates have remained stubbornly high for the past decades in small cell lung cancer (SCLC) because of having no standard targeted therapies with confirmed advantages at present. Poly [ADP-ribose] polymerase (PARP) inhibitors have shown promise in preclinical models but have had unsatisfactory clinical results in SCLC. By RNA-seq and isobaric tags for relative and absolute quantification (ITRAQ), we revealed that PARP1 inhibition led to the relocalization of forkhead box-O3a (FOXO3a) from nuclear to cytoplasm. By performing co-Immunoprecipitation (co-IP) and CRISPR-Cas9-mediated knockout plasmid we showed that FOXO3a was subject to exportin 1 (XPO1)–dependent nuclear export. We demonstrated the effects of the PARP inhibitor BMN673 on apoptosis and DNA damage were markedly enhanced by simultaneous inhibition of XPO1 in vitro. The combination of BMN673 and the XPO1 inhibitor selinexor inhibited primary SCLC cell proliferation in mini-patient-derived xenotransplants (miniPDXs) and markedly inhibited tumor growth without significant toxicity in xenograft models. The efficacy was enhanced for more than 2.5 times, compared to the single agent. Based on these findings, we further designed a novel dual PARP-XPO1 inhibitor and showed its effectiveness in SCLC. In this work, we illustrated that combining a PARP inhibitor with an XPO1 inhibitor is associated with significantly improved efficacy and tolerability. Dual PARP-XPO1 inhibition restored the FOXO3a balance and activity in SCLC. Collectively, targeting PARP1 and XPO1 opens new avenues for therapeutic intervention against SCLC, warranting further investigation in potential clinical trials.

## 1. Introduction

Small cell lung cancer (SCLC) is an extremely aggressive form of lung cancer, with key features including strongest proliferative capacity and the worst prognosis among lung cancers. Currently, platinum-based combination chemotherapy has remained the standard of care for the first-line treatment of SCLC, with the option of concomitant radiation therapy. However, the standard treatment can only achieves a poor 5-year survival rate of 6% [1]. Different from non–small cell lung cancers (NSCLC), SCLC has no standard targeted therapies with confirmed advantages at present. Therefore, the development of more precise and effective solution in the direction of targeted therapy for SCLC represents an urgent need.

While targetable genomic aberrations are very rare in SCLC, this tumor almost universally harbors inactivation of TP53 and Rb1 genes [2]. The defects of TP53 and RB1, as well as the abnormal activation of the oncogene MYC [3] and deletion of tumor suppressor gene MAX [4], make SCLC proliferate rapidly and therefore cause replication pressure. In this context, the survival of SCLC cells depends on the complete DNA damage repair (DDR) pathway [5]. Poly [ADP-ribose] polymerases (PARPs) are a family of nuclear protein enzymes involved in DDR. Targeting PARP activity can supplement the molecular defects of DDR and potentially target the most critical genetic characteristic, especially in SCLC [6–10]. Present early stage clinical trials have tried to combine PARP inhibitors with chemotherapies in SCLC [11–14]. But none of these regimens obtained positive results in the medium overall survival (OS). An important consequence of this is the generation of DNA double-strand breaks (DSB) that would normally be repaired by the homologous recombination repair (HRR) pathway. Although deficiencies in BRCA1 and BRCA2 are the most investigated examples that lead to increased PARP inhibitor activity, mutations of BRCA only occurs in 3% of SCLC patients [2]. Therefore, identifying resistance mechanisms and reasonable solutions to improve efficacy is critical.

It has been reported that PARP inhibition leads to multiple kinases activation [15–19], including PI3K/Akt, mTOR, ERK and AXL. The forkhead box-O3a (FOXO3a) is phosphorylated by activation of Akt, ERK [20] or IκB kinases (IKKs) [21], resulting in tumor progression [22]. It has been reported that the dual PARP and PI3K inhibition is accompanied by ERK activation [23], resulting in phosphorylation of transcription factors in the nucleus. Therefore, inhibition of one pathway does not prevent phosphorylation of FOXO3a by other pathways [24–26]. Phosphorylation of FOXO3a leading to relocalization to cytoplasm and loss of regulation in apoptosis and DNA repair as a transcription factor. This suggests that PARP inhibitors combined with FOXO3a upstream pathway inhibitors may not be a good strategy.

In this study, we revealed by isobaric tags for relative and absolute quantification (ITRAQ) that under PARP inhibitor treatment in SCLC, there was a selective relocalization of FOXO3a from the nucleus to the cytoplasm. We showed that this relocalization depends on exportin 1 (XPO1), which was a dependent vehicle of FOXO3a. When shuttling from the nucleus to the cytoplasm, the transcription factor FOXO3a lost its function in the regulation of apoptosis, DNA damage and autophagy. Finally, we showed that pharmacological inhibition of XPO1 (selinexor, approved by the FDA) enhances PARP inhibition in cell lines and patient xenotransplant models of SCLC. We further designed a novel compound with dual inhibition activities targeting both PARP and XPO1 and presented result of its efficacy. The results provide a strong rationale for the clinical investigation of this dual target inhibition treatment in SCLC patients.

## 2. Materials and methods

### 2.1. Cell lines, drug and antibodies

Human SCLC cell lines H69 were purchased from Cell Resource Center, Institute of Basic Medical Science CAMS/PUMC. Cell lines H69, H82, DMS114, SW1271, SHP-77, H196, H1688 were provided by American Type Culture Collection (ATCC). All cells were grown in suggested medium supplemented with fetal bovine serum and penicillin/streptomycin. All cell lines were authenticated by STR profiling.

For FOXO3a-related cell lines, SCLC cell lines were transfected with pcDNA3.1 HA-FOXO3a (TM/WT) plasmid which was carried out using Lipofectamine 3000 (Invitrogen). TM wa a triple mutant form of FOXO3a in which all three Akt phosphorylation sites were mutated to alanine (FOXO3a-TM, T32A/S253A/S315A). After 48 h, positive cells were selected with ampicillin and collected for use in experiments afterwards.

Talazoparib (BMN673) was obtained from MCE company (HY-16106), and selinexor was purchased from Selleck (S7252). Anti-PARP1 and XPO1 antibodies were purchased from Santa Cruz Biotechnology (sc-74470, sc-74454) for the Western blotting and from Sigma-Aldrich (HPA045168, HPA042933) for immunohistochemistry. Antibodies for p53 (sc-126) and Rad51(sc-53428) were purchased from Santa Cruz Biotechnology. All other antibodies were purchased from Cell Signaling Technology and abcam: FOXO3a (#12829), FOXO1 (#2880), Akt (#4691), phospho-FOXO1 (Thr24)/FOXO3a (Thr32) (#9464), phospho-Akt(#4060), (histone H3 (#4499), phosphor-histone H2A.X (#9718), HA-tag (#3724), Ki-67 (#9449), cleaved-caspase-3 (#9661), MLH1 (ab92312), MSH2(ab227941), MSH6(ab92471), PMS2(ab110638).

### 2.2. Immunohistochemistry

In total, 98 SCLC patients seen between 2008 and 2017 were included in the study, and all these patients received surgery as a first-line treatment. The study was approved by the Tianjin Medical University Cancer Hospital and Institution Ethical Committee. Briefly, paraffin sections were first deparaffinized with 100% xylene, and rehydrated with concentration gradient ethanol. To inactivate endogenous peroxidase, sliders were incubated with 3% hydrogen peroxide ($H_2O_2$) in the dark for 20 min. Antigen retrieval was performed by decloaking chamber heating in corresponding antigen repair buffer, followed by overnight incubation with primary antibodies. Slides were washed and treated with antibody signal enhancer and secondary antibody for 30 min and then conjugated with HRP and Cardassian DAB Chromogen. Two independent observers determined the percentage of cells being stained and interpreted the results in a blinded fashion. Analysis of IHC results was determined by 2 independent observers in a blinded fashion.

### 2.3. Western blotting analysis and subcellular fractionation

Proteins were prepared using Cell Lysis Reagent (Sigma, C2978) with protease and phosphatase inhibitors cocktail (Sigma, P8340). The nuclear and cytoplasmic fractions were extracted by the NE-PER Nuclear and Cytoplasmic Extraction Reagents (#78833, Thermo Scientific) according to manufacturer's protocol. The protein concentration was quantified using BCA assay (Solarbio, PC0020). Equal amounts of proteins were subjected to 10%–15% gels and transferred onto PVDF membranes. Membranes were blocked with blocking buffer [5% polyvinyl pyrrolidone PVP and 5% calf serum] for over 2 h, followed with primary antibody in 4 °C overnight. After washing, the membrane was treated with the secondary antibody for 1 h at room temperature. The proteins were detected by chemiluminescence using the Immobilon Western HRP Kit (Millipore, WBKLS0500).

### 2.4. ITRAQ

After extracted from nucleus and cytoplasm, the samples were then reduced, alkylated, trypsin-digested, and labeled following the manufacturer's instructions for the iTRAQ Reagents 8-plex kit. After the 8 labeled samples were combined, the iTRAQ-labeled peptides were fractionated by Thermo Gemini C18 columns and Thermo UltiMate

3000 UHPLC. The samples were separated on a Thermo Scientific™ EASY-Spray™ PepMap™ C18 column with a Thermo Scientific™ EASY-nLC™ 1000 HPLC system (San Jose, CA) and analyzed using a high-resolution Orbitrap Fusion mass spectrometer (Thermo Fisher Scientific, Waltham, MA).

Mass spectrometry data in RAW format were acquired by mass spectrometer. The RAW file was converted into mascot generic format (MGF) file. The MGF file and protein retrieval library were inputted into the Mascot for protein retrieval. Quality control analysis is carried to judge whether the data is qualified. Then iTRAQ quantitative analysis was carried out to screen out the significant difference proteins. The mass spectrometry proteomics data have been deposited to the ProteomeXchange Consortium via the PRIDE [27] partner repository with the dataset identifier PXD019321.

### 2.5. Immunofluorescence

Approximately $3 \times 10^4$ adherent cells were plated onto coverslips in 12-well plate. Cells on the coverslips were fixed with 4% para-formaldehyde for 15min, washed with PBS, and then permeabilized using PBS containing 0.5% Triton X-100 (PBST) for 20 min. The cells were blocked in 5% goat serum for 30 min, followed by primary antibody for 1 h at room temperature. After washed 3 times, the cells were incubated with 1:100 of the secondary antibody for 1 h. The cells were treated with 1:1000 1 mg/mL DAPI for 5 min and then mounted by Antifading mounting medium.

### 2.6. CRISPR activation

Briefly, sgRNA sequences (see Supplementary Table 2) targeting promoters of XPO1 were obtained from the sgRNA design tool (http://sam.genome-engineering.org/database/, Cas9-Activators with SAM, accessed 12/2015) and cloned into lentiCRISPRv2. Lentiviral particles. Target cells were transfected with lentiviral particles followed by Puromycin selection (1 μg/mL).

### 2.7. Apoptosis assay

Cells were treated with single or combined drugs for 36 h. Apoptotic cells were staining with annexin V-FITC/PI (BD Pharmingen™ 556547) and analyzed by flow cytometry. The results represented the mean ± SD of triplicates measurements.

### 2.8. Chromatin immunoprecipitation assay

Chromatin immunoprecipitation (ChIP) assay was performed by using the SimpleChIP Kit (CST) according to manufacturer's protocol. Briefly, approximately $5 \times 10^6$ SCLC cells, transfected with FOXO3a-HA-WT plasmid for 48 h, were exposed to single or combined drugs for 24 h in the plate and then fixed with formaldehyde. The cross-linked DNA complexes were sheared to 200–1000 base pair fragments and immunoprecipitated with anti-HA, anti-histone H3 or IgG control antibody as positive and negative control. The immunoprecipitated DNA was then purified and amplified by qPCR using SYBR green. Primers sequences are listed in Supplementary table 2.

### 2.9. RNA isolation qRT-PCR

Total RNA was isolated using the Trizol reagent according to the manufacturer's instructions. Quantitative real-time PCR (qPCR) was performed using Real-Time PCR System (Bio-Rad CFX96) and the SYBR Green PCR Mix (Takara RR820). Primers used to analyze mRNA levels were listed in Supplementary Table 2. Data were normalized to GAPDH levels and were presented as mean ± SEM and significance was calculated by unpaired Student's t tests.

### 2.10. Immunoprecipitation

Proteins were extracted using Cell Lysis Reagent (Sigma, C2978) with protease and phosphatase inhibitors cocktail (Sigma, P8340). The cell lysates were collected by centrifugation at 13 000 g for 15 min at 4 °C. Then, the immunoprecipitation was performed according to the protocol of the Dynabeads Protein A immunoprecipitation kit (Invitrogen, 10006D). Briefly, antibodies were added to the Dynabeads Protein A, and allowed to bind to the magnetics beads via their Fc-region during a short incubation. The tube was placed on a magnet, and the beads adhered to the side of the tube facing the magnet, allowing easy removal of the supernatant. The bead-bound Ab was then used for immunoprecipitation of the target antigen (Ag). The samples containing the antigen were added, and the sample was gently pipetted to resuspend the magnetic bead-Ab complex. After incubating and washing, the bead-Ab-Ag complex was eluted with elution buffer. The precipitant complexes were dissolved with $4 \times$ SDS loading buffer and analyzed by Western blotting assay.

### 2.11. Xenograft study

H196 SCLC cells ($1 \times 10^7$/mouse in 0.1 mL with 25% Matrigel and 75% saline) were subcutaneously injected into the groins of 6-week-old female BALB/c nude mice. Tumor volume was measured once every other day: Volume = 1/2 (Length $\times$ Width$^2$). Sample size was selected according to previously observed statistical variance encountered. Mice which bear tumor (average size>100 mm$^3$) were randomly separated into four groups (7 mice/group) and treated with either vehicle control or talazoparib alone (0.3 mg/kg, i.p., everyday), selinexor alone (15 mg/kg, i.p., once a week, on days 15,22, 28), or their combination. After 21-day treatment, tumor tissues and organs were harvested for further analysis. The animal experiment was conducted under an approved from the Animal Care and Use Committee of Tianjin Cancer Institute & Hospital of Tianjin Medical University.

### 2.12. Generation of a mini-PDX animal model

Human SCLC tissue samples were collected from patients diagnosed as SCLC pathologically. Patient biospecimens and information were collected under the ethical approval made by Tianjin Medical University Cancer Hospital and Institution Ethical Committee. Primary SCLC cells were extracted from tumor tissues after morselized and digested. After centrifuged and washed, cells were filled into OncoVee® capsules (LIDE Biotech Inc.), which were implanted subcutaneously via a small skin incision with 3 capsules per mouse (5-week-old BALB/c nude mouse) [28,29]. The special capsule could let in the small molecular drugs and cytokines from the microenvironment but could not let the tumor cells out. Mice were treated with the indicated drugs or vehicle, respectively for 7 days. Thereafter, the implanted capsules were removed, and tumor cell proliferation was evaluated using ATP luminescent cell viability (G7571, Promega, Madison, WI, US). Tumor cell growth inhibition (TCGI) (%) was calculated using the formula:

$$TCGI(\%) = 100\% \times$$
$$\{1 - [(Treatment\ RLU\ day7 - day0)/(Vehicle\ RLU\ day7 - day0)]\}$$

The animal experiment was conducted under an approved from the Animal Care and Use Committee of Tianjin Cancer Institute & Hospital of Tianjin Medical University.

### 2.13. Statistical analysis

Survival data were calculated by Kaplan-Meier and log-rank test methods (SPSS and GraphPad Prism). The statistical significance was analyzed using the Student's t tests. In all instances, P < 0.05 was considered significant. All in vitro experiments were run in biological triplicates, except where specified otherwise.

## 3. Results

### 3.1. PARP expression and PARP inhibition promote the PI3K/Akt pathway in SCLC

To determine the relevance of PARP1 inhibition in SCLCs, we examined PARP mRNA and protein expression in SCLC. Above all, we estimated mRNA expression levels among over 1000 cancer cell lines from the Cancer Cell Line Encyclopedia (CCLE) [30], and found that SCLC cell lines had the highest PARP expression among all solid tumor types (Fig. 1A). In addition, we assessed PARP1 protein expression by IHC in 98 SCLC tissue samples (Fig. 1B). All of the patients have not received any treatment before surgery. Analysis of PARP1 staining included both the percentage of positive cells and intensity of the staining. We stratified samples according to the score as follows: 1 to 6 as PARP1-low; 7 to 12 as PARP1-high. Based on this cutoff, we found the majority of the SCLC samples expressed high level of PARP1(over 80%) (Table 1). Although there was no significant association between higher PARP1 and poorer overall survival (OS) or progress free survival (PFS) (Fig. 1C), hazard rate (HR) were both greater than 1. It suggested that high PARP1 expression was not a prognosis indicator but a risk factor in SCLC.

To figure out compensatory pathways induced by PARP inhibition, we performed RNA sequencing which measured changes in pathways including PI3K/Akt, Wnt, Hippo signaling pathways in 2 varied types of SCLC cell lines, H69 and H82, treated with either vehicle or the most effective PARP inhibitor BMN673 for 24 h. Analysis of RNA expression showed that expression of RNAs in the PI3K/Akt pathway was increased in drug-treated cell lines (Fig. 1D).

### 3.2. ITRAQ-based quantitative analysis of the proteome of nuclear and cytoplasmic fractions under BMN673 treatment

We further performed proteomic analyses by ITRAQ to observe the protein distribution in the nucleus and cytoplasm before/after BMN673 treatment. Subcellular fractions of nucleus and cytoplasm extracted from H196 SCLC cell line were subjected to proteomics with the Nuclear and Cytoplasmic Extraction Reagents. In total, 6765 proteins were identified in the nucleus and cytoplasm. With fold-change cutoff of 1.5, the expression of 89 proteins was decreased and 73 proteins increased in the nucleus, whereas the expression of 55 proteins decreased and 80 proteins increased in the cytoplasm upon BMN673 treatment (Fig. 2A). The volcano plots indicated the regulated proteins in the nucleus and cytoplasm with a minimum of 1.5-fold change combined with a $P < 0.05$ (Fig. 2B). Intriguingly, enrichment analyses by Gene Ontology (GO), 79 quantified transcription factors of BMN673 over DMSO treatment showed specific clusters whose abundance significantly shuttled the localization between the nucleus and cytoplasm (Fig. 2C). Among these transcription factors, FOXO3a, the downstream target of PI3K/Akt, exhibited a significant increase in cytoplasm and decrease in nucleus, suggesting potential importance upon BMN673 inhibition (Fig. 2D), as well as the FOXO pathway by enrichment analysis (Fig. 2E). It is worth mentioning that Gene set enrichment analysis identified several significantly enriched pathways including, mTOR, AMPK, NF-κB and MAPK (Fig. 2E), suggesting that Akt is not the only cause of FOXO3a relocation and phosphorylation. Therefore, the inhibition of PI3K/Akt might not be the best choice to maximize the PARP inhibition efficacy.

### 3.3. FOXO3a is relocalized in SCLC cell lines following PARP inhibition

For further confirmation, we performed Western blotting and showed that the phosphorylation (activation) of Akt proteins was increased in BMN673 treated cells compared to control cells. In addition, we further found that FOXO3a, affected by Akt phosphorylation, showed increased phosphorylation in protein level (Fig. 3A). To extend our observation on the relocalization of FOXO3a in PARP inhibitor-treated SCLC cells, we examined the subcellular localization of FOXO3a in four different SCLC cell lines (H196, H1688, DMS114 and SHP-77). Western blotting and IF analyses showed that FOXO3a was predominantly transferred from the nucleus to the cytoplasm in all of these cell types after BMN673 treatment for 24 h (Fig. 3B and C). The dose and time dependence studies of BMN673 for 36/48 h also showed the relocation function upon BMN673 treatment (Fig. S1A).

### 3.4. FOXO3a is an XPO1 cargo protein

After phosphorylation, FOXO3a, with a leucine-rich nuclear export signal (NES), can be identified by XPO1, form a stable complex, and transferred into cytoplasm [31,32]. The effect of XPO1 inhibition on FOXO3a transcriptional programs and functional networks/pathways likely contributes to the antitumor activity [33]. To determine XPO1 binding activity if FOXO3a remained in the nucleus nonphosphorylated, we established SCLC cell lines bearing different constructs: hemagglutinin (HA)-tagged FOXO3a-triple mutant (TM) or HA-tagged FOXO3a-WT. TM is a triple mutant form of FOXO3a in which all three Akt phosphorylation sites are mutated to alanine (FOXO3a-TM, T32A/S253A/S315A) [34]. With these mutations, FOXO3a cannot be phosphorylated by Akt, so it has transcriptional activity in nucleus. Upon treatment with BMN673, which improved phosphorylation of Akt and FOXO3a, TM of FOXO3a significantly impaired XPO1-FOXO3a interaction by co- Immunoprecipitation (co-IP), suggesting a significant role of FOXO3a phosphorylation in mediating nuclear-cytoplasm shuttling (Fig. 4A).

To determine whether the effects of relocalization on FOXO3a was XPO1 specific, we performed CRISPR-Cas9-mediated knockout of XPO1. We found by Western blotting and IF that, after knocking out of XPO1, FOXO3a expression in the nucleus was restored regardless of BMN673 treatment (Fig. 4B and C). We further demonstrated the XPO1 binding function on FOXO3a phosphorylation by co-transfection of XPO1-knockdown/WT and FOXO3a TM/WT plasmid into SCLC cell lines. The result by Western blotting and IF showed that after knocking out of XPO1, the majority of FOXO3a stayed in the nucleus, especially with FOXO3a-TM (Fig. 4D and E).

We then elucidated the effect of XPO1 selective inhibition following PARP inhibition on the nuclear–cytoplasmic transporting of FOXO3a protein. We treated four SCLC cell lines with BMN673 and an XPO1 inhibitor, selinexor (KPT-330), for 24 h and examined the subcellular distribution of FOXO3a by Western blotting and immunofluorescence. Intriguingly, selinexor treatment, combined with BMN673 for 24 h, resulted in a significant relocalization of FOXO3a, FOXO1 proteins in the nucleus and cytoplasm, leading to nuclear accumulation (Fig. 4F and G). The dose and time dependence studies of the combination at 12/36 h also showed the relocalization function (Fig. S1b).

To confirm whether the synergistic function of the BMN673 combined with selinexor is greater than present PARP + PI3K/Akt inhibitor regimens, we performed MTT assays with 3 varieties of PI3K inhibitor buparlisib, alpelisib and copanlisib, and Akt inhibitor capivasertib. We observed that our regimen had the greatest efficiency (Fig. S1c). The levels of synergism and combination index (CI) were calculated using CompuSyn software (Fig. S1d). We stratified synergistic effect according to the CI values as follows: <0.1 as very strong synergism; 0.1–0.3 as strong synergism; 0.3–0.85 as synergism; 1.45 to 3.33 as antagonism [35]. Based on this cutoff, we found both cell lines (H196 and SBC-2) expressed very strong synergism (0.09 and 0.07) by treating with BMN673 and selinexor. Moreover, to prove the drug toxicity of the combination on normal cells, we performed CCK8 assays on Peripheral blood mononuclear cell (PBMC) separated from human peripheral blood. The results indicated that our regimen PARP + XPO1 inhibition expressed the least toxicity (Fig. S1e).
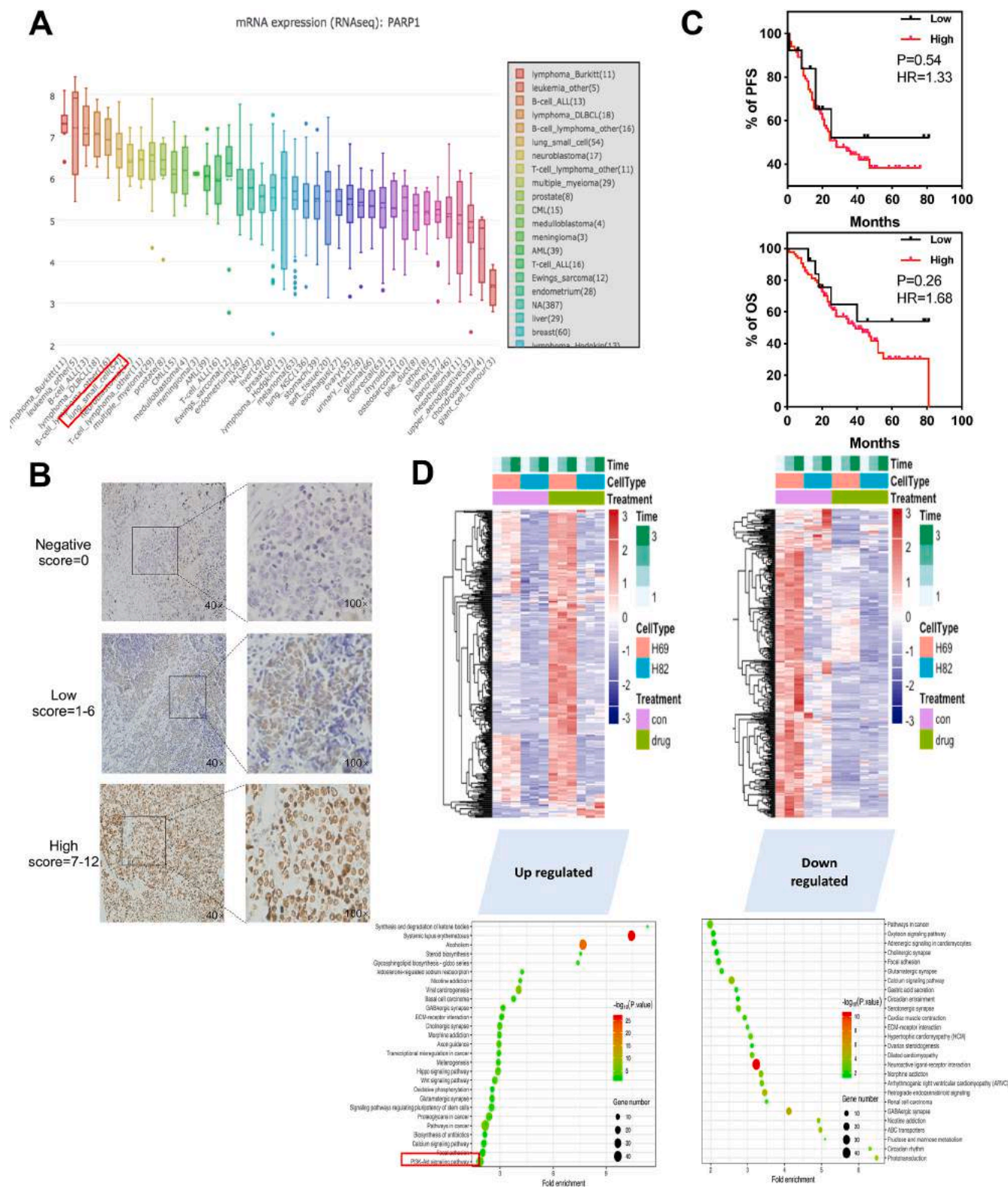
**Fig. 1.** PARP expression and PARP inhibition promotes the PI3K/Akt pathway in SCLC. (A) SCLC Ranked the top of PARP1 mRNA expression in all kinds of solid tumors in the CCLE. **(B)** Representative images of PARP1 IHC staining at different levels of expression in SCLC. **(C)** Patient survival curves plotted according to the PARP1 expression levels (PARP1-high versus PARP1-low) in SCLC at all stages. **(D)** Hierarchical clustering of all the quantified genes based on the ratios of drug treatment. Columns represent different samples. Rows represent quantified genes. Bubbles plots showing up/downregulated pathways by drug treatment.

**Table 1**
Clinical characteristics and PARP1 expression of 98 SCLC patients.

| Characteristics | Patients Population (N = 98) | | PARP1 High Class (N = 98) | | P Value |
|---|---|---|---|---|---|
| | NO. | %Total | NO. | %Sub-class | |
| Ages(years) | | | | | |
| ≤60 | 40 | 40.82% | 35 | 87.5% | 0.853 |
| >60 | 58 | 59.18% | 50 | 86.21% | |
| Gender | | | | | |
| Male | 16 | 16.33% | 14 | 87.5% | 0.921 |
| Female | 82 | 83.67% | 71 | 86.59 | |
| Smoking History | | | | | |
| Yes | 13 | 13.27% | 12 | 92.31% | 0.525 |
| No | 85 | 86.73% | 73 | 85.88% | |
| VALSG Stage | | | | | |
| Limited | 82 | 83.67% | 74 | 90.24% | 0.993 |
| Extensive | 16 | 16.33% | 11 | 68.75% | |
| AJCC 7th Stage | | | | | |
| I-II | 55 | 56.12% | 48 | 87.27% | 0.823 |
| III-IV | 43 | 43.88% | 37 | 86.05% | |
| Type | | | | | |
| Pure (PSCLC) | 6 | 6.12% | 5 | 83.33% | 0.135 |
| Combined (CSCLC) | 92 | 93.88% | 80 | 86.96% | |
| PARP1 Status | | | | | |
| Low | 13 | 13.27% | | | |
| High | 85 | 86.73% | | | |

### 3.5. Combination of selinexor and PARP inhibitors results in the induction of apoptosis in SCLC cells in vitro

To examine the synergistic effect of selinexor and PARP inhibitors on cell apoptosis, 5 SCLC cell lines were treated with indicated drugs for 36 h. Induction of apoptosis was calculated by annexin V-FITC and PI of 5 cell lines showing increased apoptosis in the combinational treatment versus either drug alone (Fig. 5A and B). Sensitive cell lines exposed to the combination of BMN673 and selinexor, except SW1271 cell line, showed a significantly increase in the proportion of apoptotic cells compared to that in the control cells (Fig. 5C).

To further evaluate the effect on cell apoptosis of the combination, we investigated the possible mechanisms by which selinexor and BMN673 may regulate Bim, FasL and Trail [36–38]. A significant induction of proapoptotic Bim, FasL and Trail, which are transcriptionally regulated by XPO1 cargoes, FOXO3a [39,40], was also observed in H196 and H1688 cell lines using ChIP assay (Fig. 5D). Furthermore, similar increase of Bim, FasL and Trail mRNA level was observed in other 2 SCLC cell lines using real-time PCR (Fig. 5E). Thus, we reasoned that the combination may upregulate Bim, Fasil and Trail by targeting FOXO3a. In consistence with annexin V assay, we detected a clear cleavage of PARP1(C-PARP-1) in the combination treatment, but not in every single drug treatment in the SCLC cell lines (Fig. 5F).

### 3.6. Combination of selinexor and PARP inhibitors reduces expression of DNA damage repair genes

In addition to PARP inhibition-induced cytoplasm restoration, we hypothesized that other mechanisms may explain the combinatorial effect of selinexor and BMN673. High-throughput sequencing studies on protein expression in tumor cells revealed that several DDR proteins were downregulated affected by selinexor treatment [41,42]. This conclusion was verified by the observation that the indicated treatment of 4 SCLC cell lines resulted in significantly reduction in DNA damage repair protein levels. These included the DNA damage response protein Chk1 [43,44] and DNA damage repair protein Rad51 [45–47]. The mismatch repair (MMR) enzymes, MSH2, MLH1, PMS1 and MSH6, correct DNA mismatches and small insertions/deletions during DNA replication and homologous recombination (HR) [48]. The combination of selinexor and BMN673 synergistically reduced the expression of DNA damage repair genes MSH2, MLH1, MSH6 and PMS2 at the protein level (Fig. 6A) and inhibited the mRNA levels of these genes (Fig. 6B) after 24 h.

Of note, the exhaustion of DNA damage repair proteins in combination-treated cells significantly increased Ser 139-phosphorylated H2AX histone (γH2AX), a marker of DNA damage, as indicated by Western blotting and IF. In addition, the expression of Rad51, a marker of DDR, decreased more potently for 5–20 times with the combination than with any of the single agent (Fig. 6C).

### 3.7. XPO1 inhibition increases BMN673 sensitivity and survival in SCLC tumor–bearing mice

To explore the in vivo effect of the BMN673 and selinexor combination, xenotransplant mouse models were established using H196 SCLC cells. Based on our findings, mice treated with the combination were significantly smaller at the tumor size after 21-day treatment than those treated with DMSO or each single drug (P < 0.05; Fig. 7A–C). Importantly, combination treatment was well tolerated with a weight loss in 10% compared with single-agent treatment and the control group (Fig. 7D). Hematoxylin-eosin (HE) staining further revealed no evidence of toxicity in liver and kidney (Fig. 7E). Moreover, the BMN673 + selinexor combination significantly eliminated the expression of the proliferation marker Ki-67 and increased the expression of the apoptosis marker cleaved caspase-3 (P < 0.05; Fig. 7F).

Because both of the drugs are not yet approved for SCLC, we performed in vivo examination in 6 miniPDX samples derived from 6 SCLC patients as described in method (Table S1). The tumor cell proliferation was evaluated using ATP luminescent cell viability. Compared with normal PDX model, miniPDX model can yield results faster (in 7 days) and have a positive predictive value of 92%, which is gradually used in drug development research. We generated sufficient primary tumor cell-bearing mice to examine the effect of the selinexor + BMN673 combination for 7 days. After that, tumor cell proliferation was analyzed as previously described. As expected, it showed that the compared with each single agent or control, the combination of BMN673 and selinexor significantly reduced the relative proliferation rate of tumor cells (T/C %) in 5 patients (Fig. 7G). Furthermore, the combination was even more effective than the standard chemotherapy regimens in SCLC in 3 s-line patients (Fig. S1F).

Based on the above promising results, we further developed a novel dual compound DIR-639 targeting PARP and XPO1 (Fig. S2a). The detailed synthesis process is explained in the supplementary materials and methods. We examined its effects by MTT and got preliminary results of its efficiency (Fig. S2b) across all the cell lines, including the insensitive cell line SW1271. Moreover, we performed a cellular PARP assay to and determined that PARP enzymatic activity was affected at approximately 40 nM (Fig. S2c). The DIR-639 treatment led to a significant restoration of FOXO3a, FOXO1 and p53 in the nucleus (Fig. S2d, e). This suggests that the new drug DIR-639 has promising clinical value in patients, which needs further investigation. Therefore, we raised the model that PARP inhibition induced relocation of FOXO3a in cytoplasm and depending on XPO1 activity (Fig. 8). Combination of PARP inhibitor and XPO1 inhibitor is a promising regimen for treating of SCLC.

## 4. Discussion

PARP inhibition is a novel and potential therapy in SCLC. PARP protein levels are upregulated in SCLC compared to other lung cancers [8]. We confirmed that PARP1 is overexpressed at both the mRNA and protein levels in SCLC samples and cell lines, which is consistent with previous studies. Although high expression of PARP1 is not a prognosis marker according to our study, hazard ratio (HR) indicated that high PARP1 expression is an essential risk factor. The results of previous
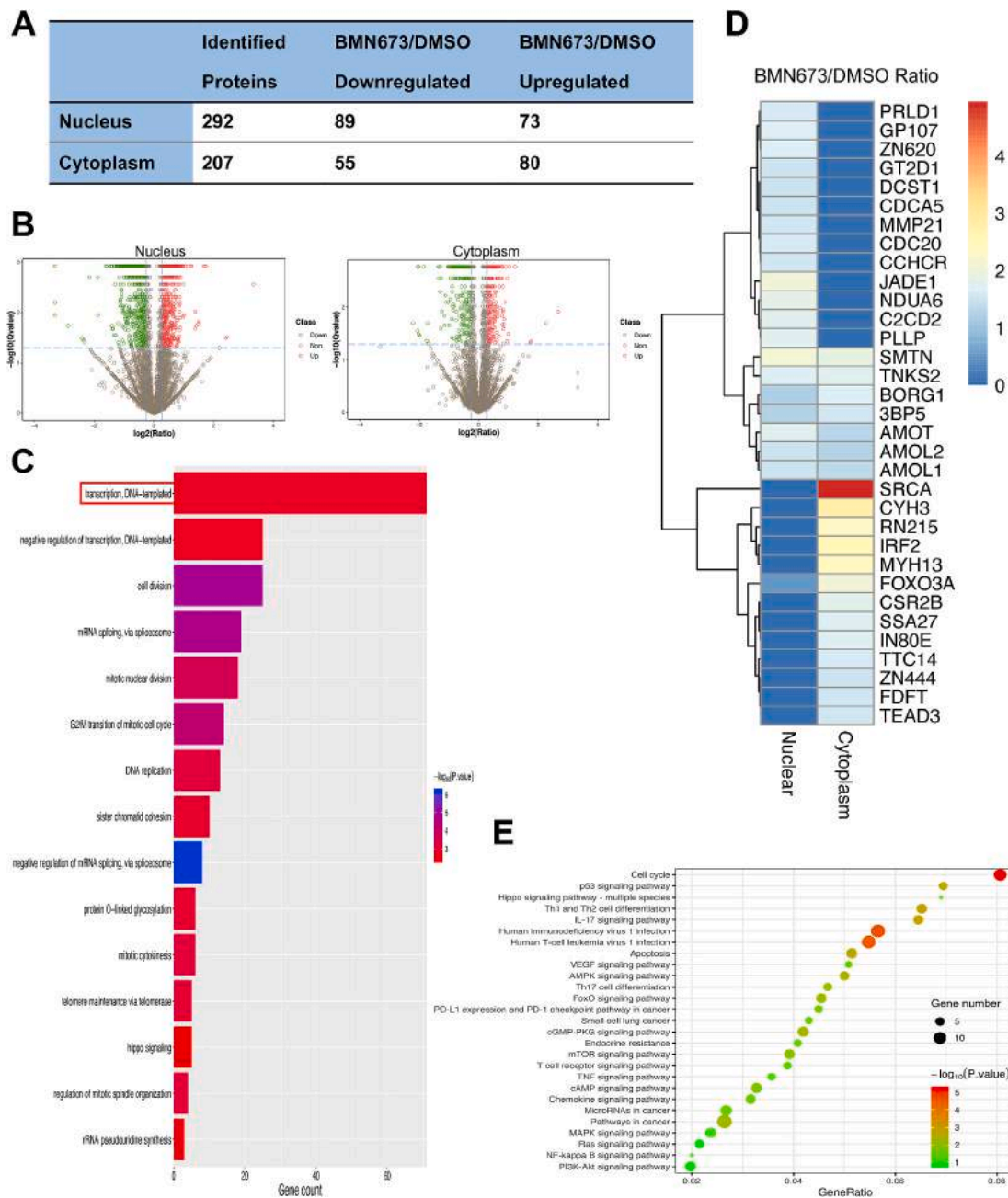
**Fig. 2.** ITRAQ-based quantitative proteomics of nuclear and cytoplasmic fractions in SCLC cells affected by BMN673. (A) Number of proteins identified from nuclear and cytoplasmic subcellular fractionation of NCI–H196 cells and the number of proteins with a 1.5-fold change upon BMN673 treatment. **(B)** Volcano plot representing the difference of protein changes in expression in the nucleus or cytoplasm between DMSO and BMN673 treatment. Log$_2$ ratios of the fold changes are plotted versus log$_{10}$ of the P values derived from a *t*-test. Proteins with a minimum of 1.5-fold change and a P value smaller than 0.05 were considered significant. Blue dots, downregulated proteins; red dots, upregulated proteins. **(C)** Gene Ontology (GO) enrichment analysis of different expressed proteins upon BMN673 treatment. **(D)** Hierarchical clustering of all the genes based on the ratios of drug treatment. Columns represent different subcellular fractions. Rows represent quantified genes. **(E)** Bubbles plots showing enriched protein-protein interaction pathways analyzed by KEGG.

studies showed that SCLC cell lines are sensitive to PARP inhibitors and provided preclinical confirmation that PARP inhibition enhances the anticancer activity of chemotherapy by downregulating key DDR mechanisms. Clinical trials of a number of PARP inhibitors, in a variety of combinations, are ongoing in patients with SCLC. However, patients did not get obvious benefits in median PFS (6.1 m vs. 5.5 m) and median OS (10.3 m vs 8.9 m) [11,13]. The mechanism of PARP inhibitors in SCLC appears to be different, while in ovarian and breast cancer, sensitivity is in large part driven by BRCA mutations or other mutations in genes regulating HR [6,49]. In SCLC, however, where BRCA mutations are rare occurred (3–4%) [2,8], the great majority of patients do

not get benefit from them. Most of the PARP inhibitors combinations attempted recently involve DNA damaging chemotherapies, some of which might have overlapping mechanisms of actions (MoA) with PARP inhibitors. Therefore, the efficacy may be limited by shared mechanisms of resistance [50].

It has been reported in a previous study that resistance to PARP inhibition is correlated with the upregulation of PI3K/Akt pathway [15, 16]. PI3K pathway activation leads to the stimulation of cell growth, motility, survival, and metabolism, and also sensing of DDR [51]. We assessed this point in SCLC cell lines but got smaller CI index by MTT, compared to the combination of BMN673 and selinexor. RNA-seq was
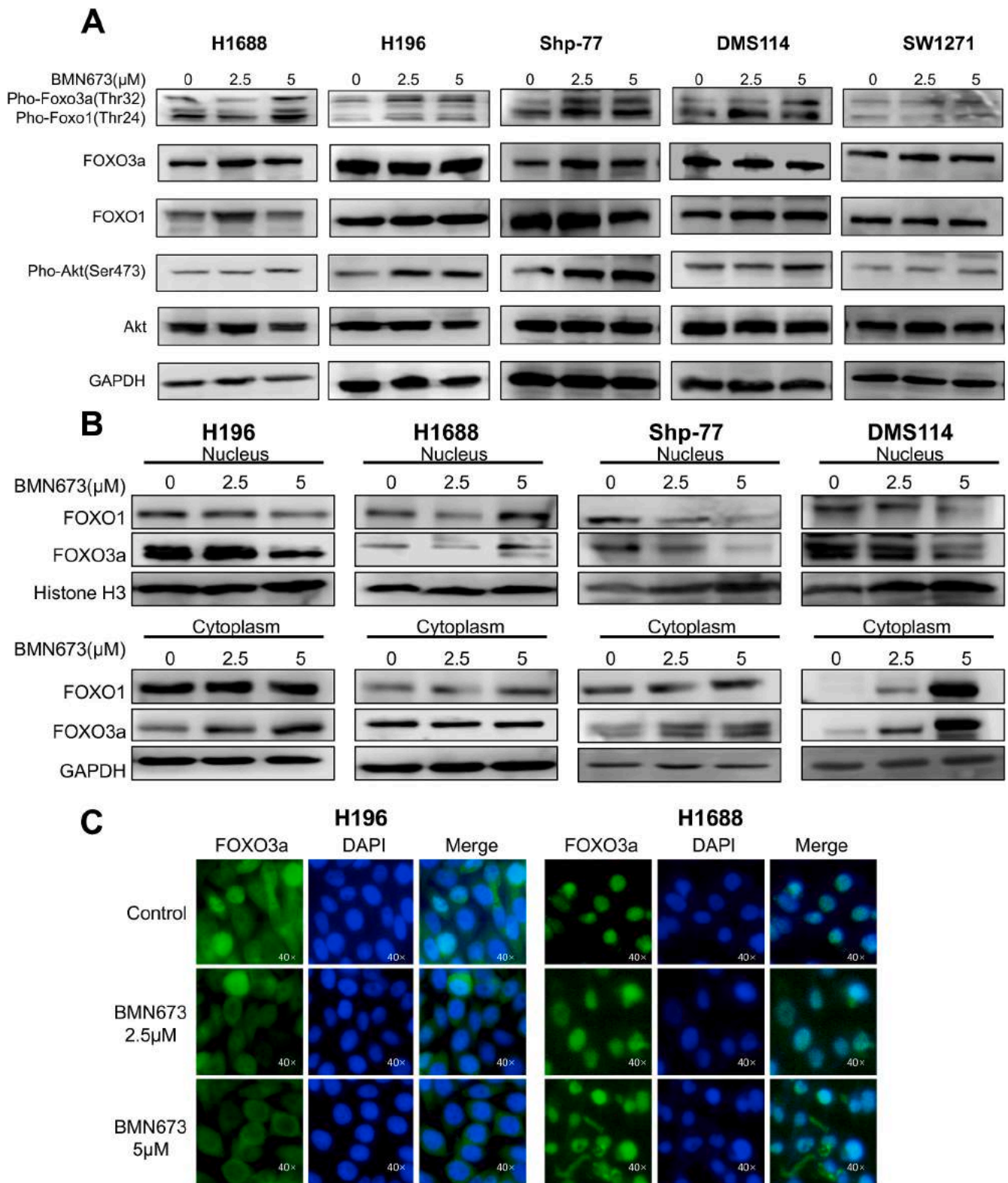
**Fig. 3.** FOXO3a is frequently relocalized in SCLC cell lines following PARP inhibition. **(A)** Individual phosphorylated proteins in the Akt pathway (p-Akt and p-FOXO1/3a) are increased following treatment with BMN673 **(B)** Western blotting detection of FOXO3a distribution in the cytoplasm and nucleus after BMN673 treatment. GAPDH and histone H3 were used to show equal protein loading and purity of cytoplasmic and nuclear fractions. **(C)** IF detection showing FOXO3a relocation in the cytoplasm after BMN673 treatment. Images were representative of at least three replicates.
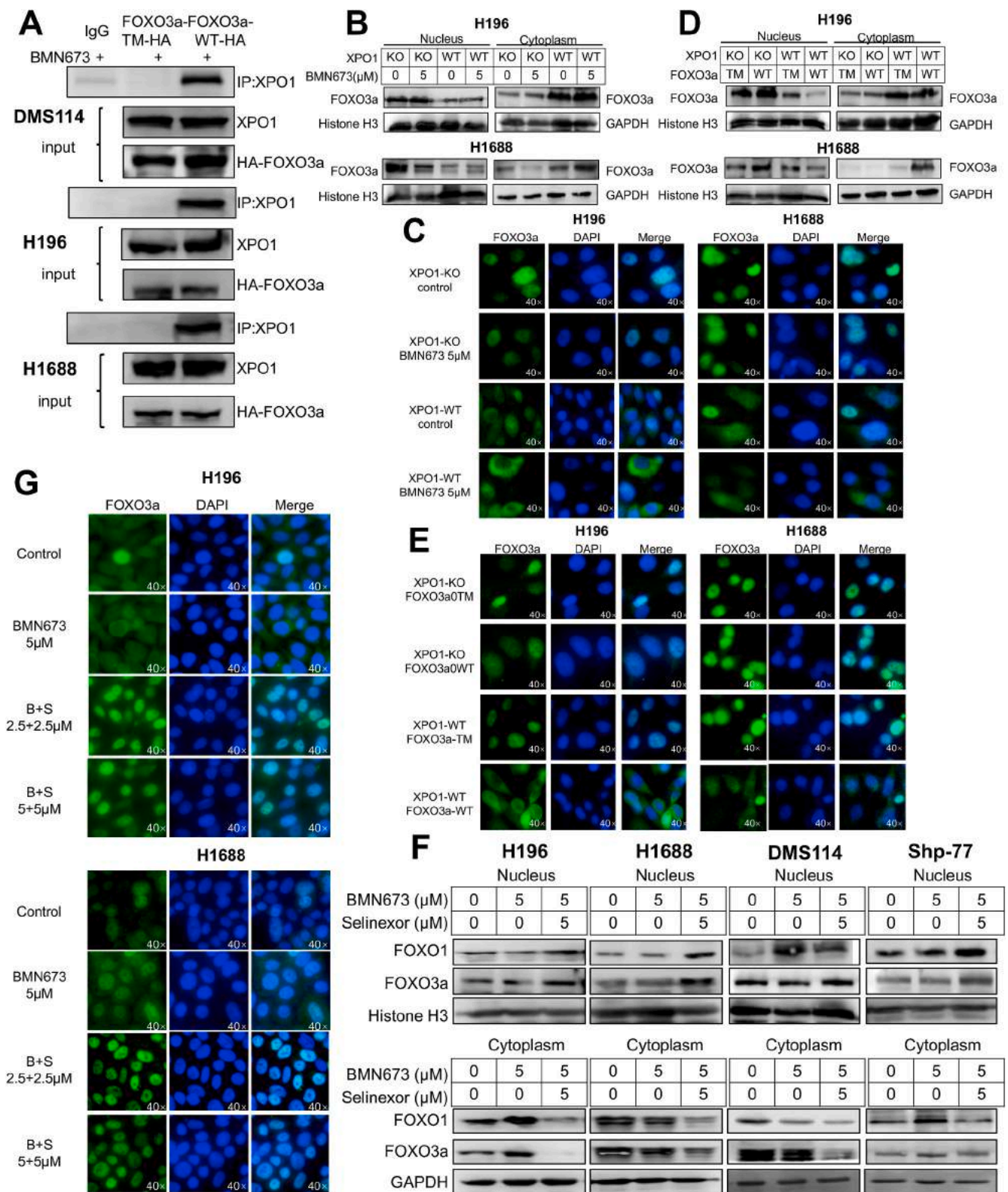
**Fig. 4.** FOXO3a is an XPO1 cargo protein. **(A)** Immunoprecipitation (IP) followed by Western blotting analysis for associated nuclear export receptor XPO1 in FOXO3a-HA-TM or FOXO3a-HA-WT SCLC cells treated as indicated. FOXO3a and XPO1 levels were also detected by Western blot in whole cell extracts (IgG). Western blotting **(B)** and IF **(C)** show the distribution of FOXO3a after XPO1 knockout and upon BMN673 treatment. Western blotting **(D)** and IF **(E)** showing the distribution of FOXO3a after co-transfection of XPO1-knockout/WT and FOXO3a-TM/WT plasmids. **(F)** Lysates under PARP and XPO1 inhibition from 4 SCLC cell lines results in increased distribution of FOXO3a as determined by western blotting. **(G)** IF analysis showing the intracellular and cytoplasmic localization of FOXO3a in proliferating H196 and H1688 cells. Images are representative of at least three replicates.
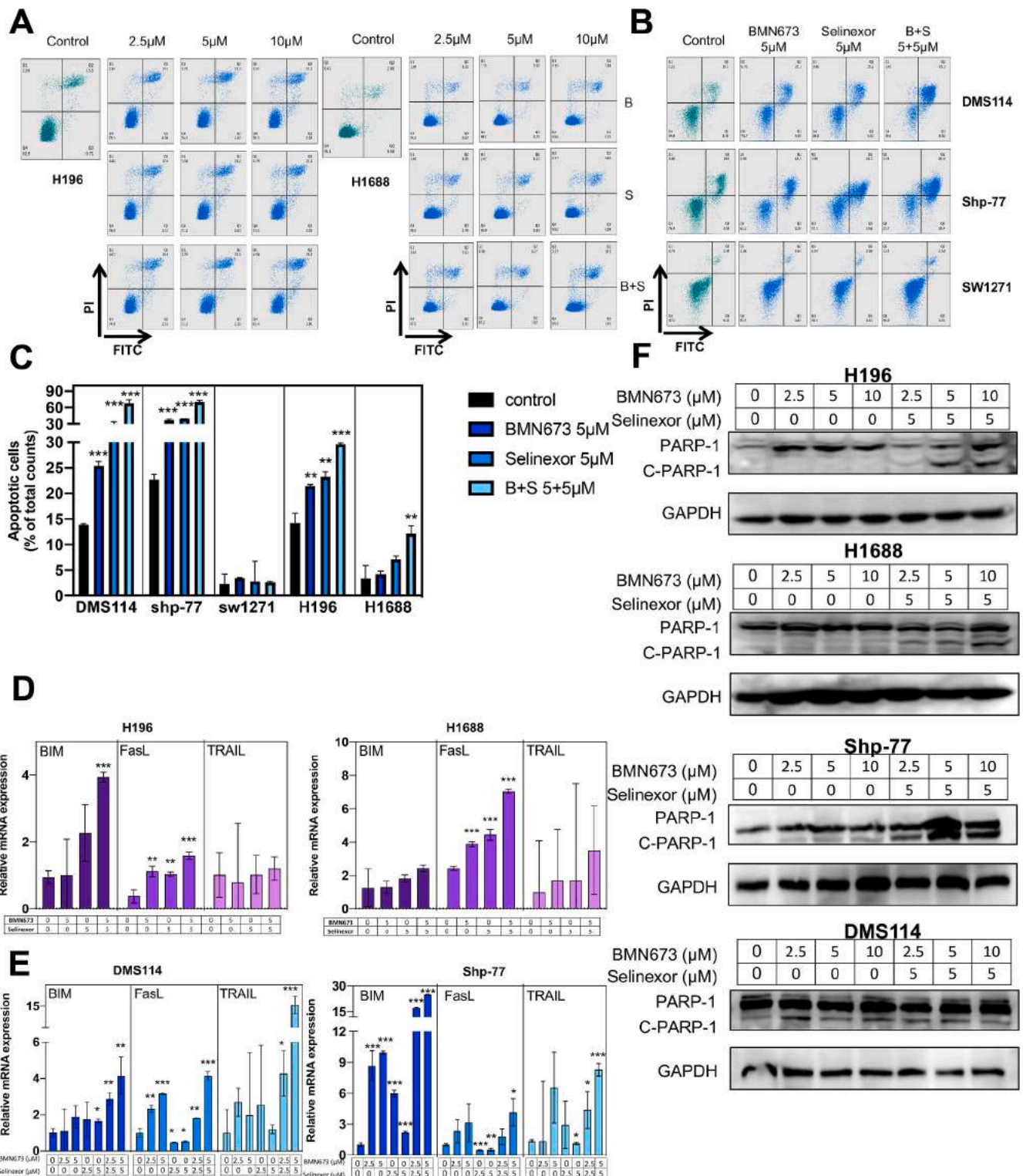
**Fig. 5.** Combination of selinexor and PARP inhibitors results in the induction of apoptosis in SCLC cells in vitro. **(A–B)** Apoptosis of 5 SCLC cell lines was determined by flow cytometry-based annexin V/PI apoptosis assay 48 h after treatment with BMN673, selinexor or the combination. Representative contour plots from each experiment are shown. **(C)** Quantification of apoptotic cells. **(D)** Total mRNA expression of Bim, FasL and Trail measured by ChIP assay after drug treatment in H196 and H1688 cell lines. An unpaired *t*-test was used to compare values of treatment groups to their respective vehicle-treated group. *P < 0.05, **P < 0.01, ***P < 0.001 **(E)** Expression levels of Bim, FasL and Trail measured by quantitative PCR extracted from DMS114 and SHP-77 cell lines 24 h after drug treatment. An unpaired *t*-test was used to compare values of treatment groups to their respective vehicle-treated group. *P < 0.05, **P < 0.01, ***P < 0.001 **(F)** Western blotting analysis of PARP1 cleavage in SCLC cells after the indicated treatment. Higher cleaved-PARP1(C-PARP-1) expression stands for improved apoptosis progress.
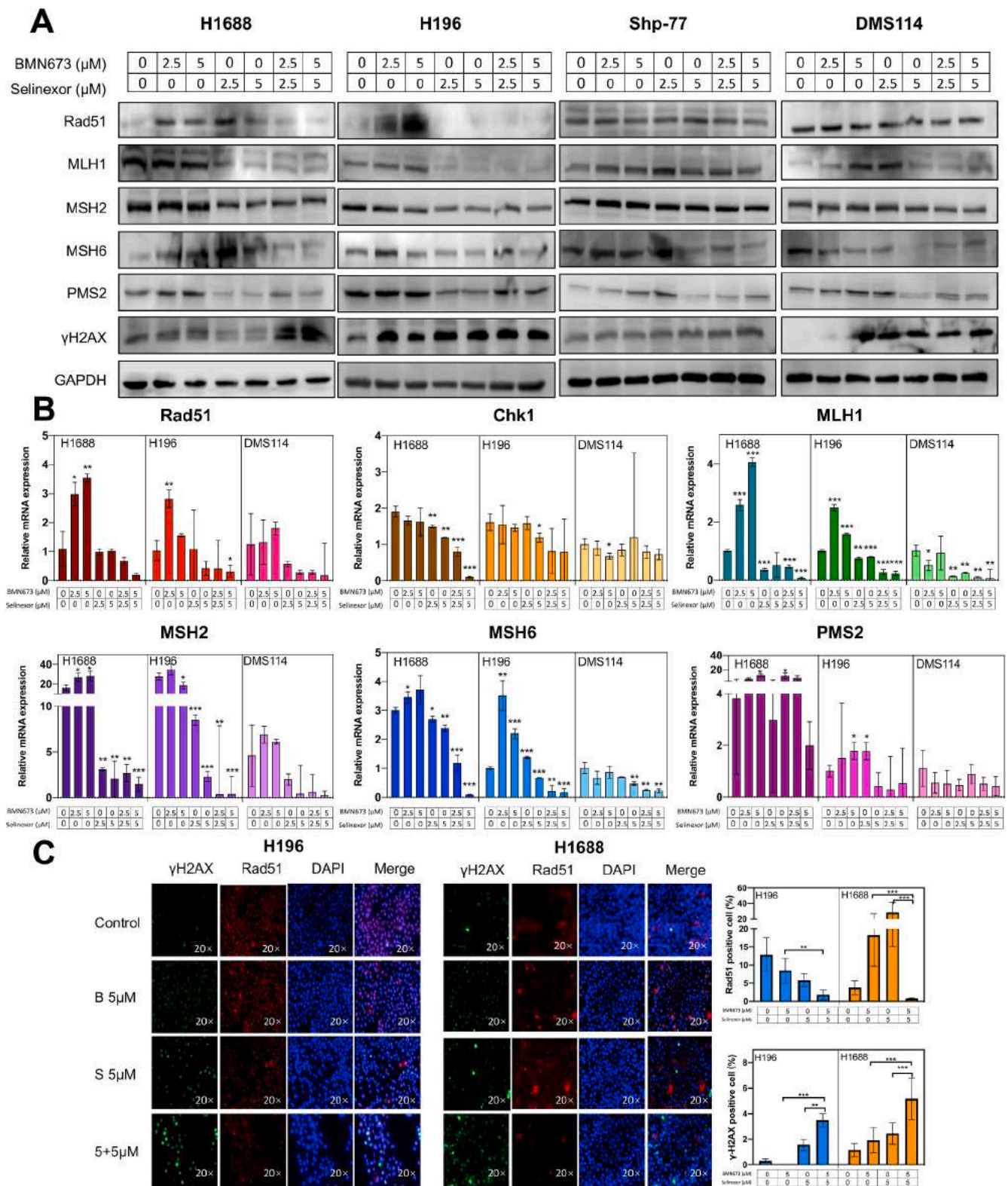
**Fig. 6.** Combination of selinexor and PARP inhibitors reduces expression of DNA damage repair genes. Protein **(A)** and total mRNA **(B)** expression of Chk1, MSH2, Rad51, MLH1, PMS2, MSH6 and γH2AX were measured by real-time PCR and Western blotting after the indicated drug treatment for 24 h in SCLC cell lines. An unpaired *t*-test was used to compare values of treatment groups to their respective vehicle-treated group. *P < 0.05, **P < 0.01, and ***P < 0.001. **(C)** Analysis by IF of γH2AX and Rad51 foci in SCLC cells after exposure to the dual-inhibition treatment for 24 h showing increased expression of increased γH2AX (3 times) and decreased Rad51(30 times). *P < 0.05, **P < 0.01, and ***P < 0.001. DAPI, 4′,6-diamidino-2-phenylindole.
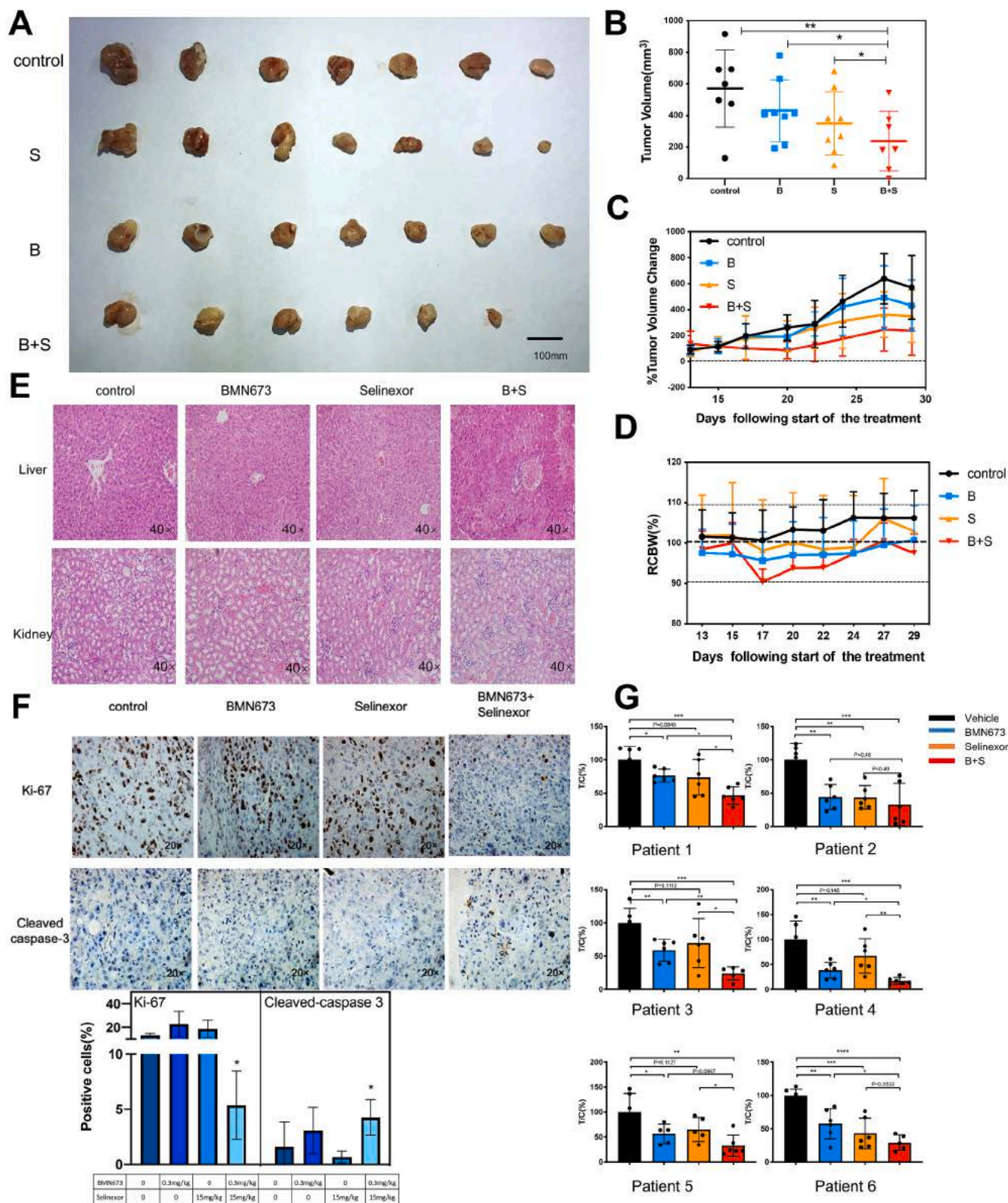
**Fig. 7.** XPO1 inhibition increases BMN673 sensitivity and survival in SCLC tumor–bearing mice. Mice bearing H196 xenografts were treated with vehicle control, BMN673 (0.3 mg/kg/day), selinexor (15 mg/kg/week) or their combination. Tumor collection **(A)** and tumor growth curve **(B and C)**. **(D)** Body weight change of mice with the indicated drug treatment restricting within 10%. **(E)** Hematoxylin and eosin (HE) histological assay of liver and kidney organs after various treatments proving tolerable toxicity. **(F)** Ki-67 and cleaved caspase 3 were analyzed in tumor tissues at the end of experiments by immunohistochemical staining. Data represent the mean ± SD, error bars represent SD. *P < 0.05, **P < 0.01, and ***P < 0.001. **(G)** Mini-PDX models were generated, and the proliferation rate of SCLC primary tumor cells was measured under the indicated drug treatment, as normalized to vehicle treatment. Combinational treatments resulted in 2.5 times reduce in cell activity compared with every single drug. An unpaired *t*-test was used to compare values of treatment groups to their respective vehicle-treated group. Data represent the mean ± SD, error bars represent SD. *P < 0.05, **P < 0.01, and ***P < 0.001.
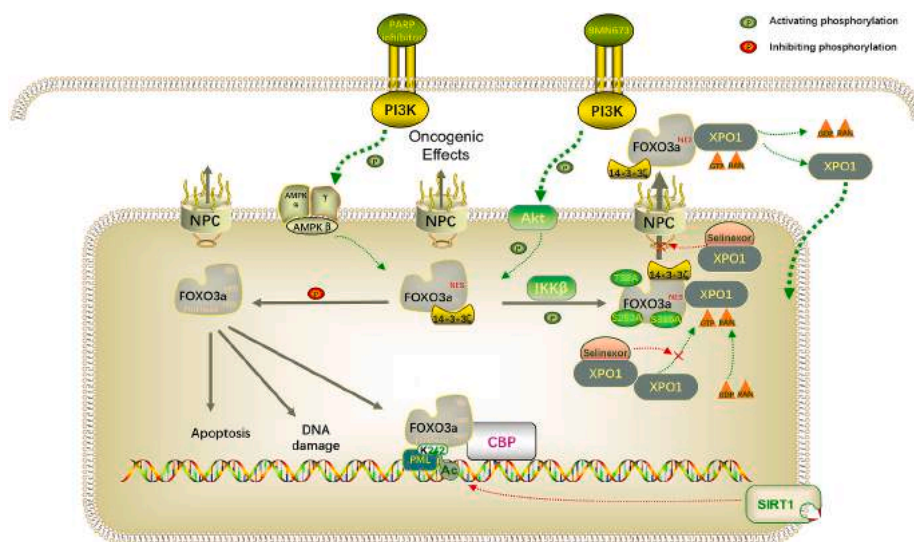
**Fig. 8.** Model of nuclear relocation of FOXO3a phosphorylation induced by PARP inhibition and mediated by XPO1 PARP inhibition drives PI3K/Akt, AMPK-ERK and IKKβ activation, followed by phosphorylation of FOXO3a. XPO1 recognizes phosphorylated FOXO3a with NES domain and exports FOXO3a from nuclear into cytoplasm. Therefore, FOXO3a loses the function of promoting the process of apoptosis and DNA damage, resulting in tumor progression.

performed after treatment with PARP inhibitor and the results confirmed those of the previous study, suggesting that SCLC may evade PARP inhibition by activation of the PI3K/Akt pathway. Clinical trials combining PARP inhibitor and PI3K/Akt inhibitors are ongoing in patients with breast and ovarian cancer [52]. The positive effect mainly occurred in patients with BRCA mutations, so other drug combinations need further exploration in SCLC. There is a common view that PARP inhibitors cause cancer cell death by eliciting an extreme level of genomic instability. Therefore, SCLC could be treated with a combination of PARP inhibitors and a targeted method that could promote programmed cell death [36].

Here, our data presented a model that PARP inhibition induced relocation of FOXO3a in cytoplasm and depending on XPO1 activity (Fig. 8). We observed by protein quantification that transcriptional function was affected under the treatment of BMN673. Among the affected factors, FOXO3a exhibited a significant increase in cytoplasmic expression and a decrease in the nucleus expression, suggesting its potential importance upon BMN673 inhibition. It has been reported that ERK phosphorylation is induced by dual PARP and PI3K inhibition [23]. The abnormal activation of PI3K/Akt and MAPK/ERK pathways can lead to the phosphorylation of FOXO3a and the suppression of transcriptional activity in cancer [25,26,53]. In addition, IKK, the upstream signal of NF-κB, can phosphorylate FOXO3a independent of Akt pathway [24, 25]. In our study, we found that MAPK, NF-κB and AMPK activation and IKKα expression increase in the nucleus upon the BMN673 treatment, as detected by ITRAQ. Therefore, only PI3K inhibitor combined with BMN673 could not prevent the activation of the important transcriptional factor, FOXO3a.

Members of the mammalian FOXO family of forkhead transcription factors are critical positive regulators of longevity in species as diverse as worms and flies [54,55]. Under normal circumstance, the survival kinase AKT is inactive, and FOXO3a is expressed in the nucleus where act on p27 and other unidentified downstream targets to induce apoptosis [56]. It is obvious that transcriptional regulation of multiple downstream targets plays crucial roles in the proapoptotic or anti-apoptotic function of FOXO. The nuclear-cytoplasmic transport of proteins is important in preserving normal cellular capacities. The nuclear export of proteins relies on the activity of transport vehicles, exportins. Exportin-1 (XPO1), also known as chromosomal region maintenance 1 (CRM1), mediates the transport of approximately 220 proteins [57–59].

XPO1 is the nuclear exporter of several tumor suppressor (TSP), growth regulatory (GRP) proteins, including FOXO family. Under physiological conditions, the export of these proteins prevents them from overacting in the absence of DNA injury or other oncogenic activities [60,61]. In cancer cells, however, this export of proteins prevents their tumor suppressor activity and boosts tumorigenesis [61,62]. Hence, targeting XPO1 inhibition could be a promising treatment method. With XPO1 knockout, FOXO3a stays in the nucleus regardless of BMN673 treatment. In addition, XPO1 knockout can restore the FOXO3a in the nucleus regardless of phosphorylation. Thus, we have generated a direct link between FOXO3a relocalization and PARP inhibitor resistance. The use of an XPO1 inhibitor can restore FOXO3a nuclear localization. Based on the data, we observed that a combination of XPO1 inhibition and PARP inhibition can alter the PARP inhibitor resistance.

Our results show selinexor combined with BMN673 induces apoptosis of SCLC cells, an important process of the antitumor activity resulting from the combination. The combination-induced apoptosis can be explained in part by the significant induction of the proapoptotic proteins Bim, FasL and Trail, which are not directly regulated by XPO1 but are transcriptionally controlled by XPO1 cargoes such as FOXO3a proteins [32,40].

In addition, preclinical studies have shown that a series of targeted drugs such as PI3 kinase signaling pathway inhibitors can cause or strengthen HR defects in tumor cells, making tumor cells more sensitive to PARP inhibitors. Another strategy is to combine PARP inhibitors with drugs that disrupt the ability of tumor cells to arrest the cell cycle. Because tumor cells need to arrest the cell cycle for DNA repair, drugs that disrupt this function may make tumor cells more sensitive to PARP inhibitors [63]. The majority of combined therapies enhance the effect of PARP inhibitors by increasing DNA damage or inhibiting DNA repair mechanisms. We observed that the combination leads to significant inhibition of the DNA damage repair genes, including Rad51 and Chk1, and consequent reduction of HR repair. This could be another mechanism to explain the combinational effect of selinexor and BMN673. Inhibiting DNA repair mechanisms in cancerous cells is currently being explored in cancers with the purpose of increasing drug sensitivity.

We further performed in vivo experiments not only in common xenotransplant mouse models using SCLC cell line, but also in miniPDX samples of SCLC. MiniPDX is a novel method generally extended to the preclinical models to rapidly obtained results for particular drugs

combination [64]. Compared with normal PDX models, miniPDX models can yield results faster (in 7 days) and have a positive predictive value of 92% [28,29]. At present, the project leaded by Shukui Qin, Establishment and Application of Large Data Platform for Individualized and Accurate Treatment, is based on PDX and mini-PDX model. The ongoing project including thousands of samples was reported on 2018 Chinese Society of Clinical Oncology (CSCO). It suggests that the mini-PDX assay is of high predictive power in preclinical studies. We have already performed studies on mini-PDX models of 6 SCLC patients and obtained positive results.

Based on our promising findings, we further developed a novel compound with dual inhibition activities targeting both PARP and XPO1 and demonstrated preliminary efficiency in SCLC. It is worth mentioning that the insensitive cell line SW1271 exhibited high susceptibility to the new agent DIR-639 with an IC50 value of approximately 2 μM in 24 h, making it much more sensitive than other cell lines. The new drug needs further exploration and verification, but the effect of the compound suggests the combination of targeting both PARP and XPO1 is a promising clinical method in SCLC. Not only the combination of two specific agents, BMN673 and selinexor, had a synergistic effect, but targeting of both PARP and XPO1 has potential interaction mechanisms, no matter the drug structure. With novel dual inhibitors, SCLC patients could experience greater efficacy, specificity, tolerability and less toxicity.

A limitation of the present study is that the molecular basis for the relocalization remains unknown. Other XPO1 cargo such as p53 relocalization has also been observed. It has been reported that there are some structural and functional similarities between p53 and FOXO3a [65]. P53 and FOXO3a can control cell cycle progression and DNA damage repair, and both can be post-translationally modified by acetylation and phosphorylation. Therefore, there is a functional crosstalk between the two transcription factors. Extending this, it is likely that XPO1 inhibitors may alter the export of multiple cargo proteins because they globally inhibit XPO1. Although this could be seen as a limitation of the drug, it is clear from the present study that the relocalization of FOXO3a alone can maximum PARP1 inhibition efficacy. Moreover, although the preclinical data are strongly supportive of both efficacy and acceptable toxicity, we have not yet demonstrated the activity and tolerability of the combination in human patients. Finally, the novel compound we designed needs further investigation. After optimizing structure, comparing effect, testing in vivo effect and toxicity, we still have a long way to go for clinical use.

## 5. Conclusions

In summary, we demonstrated the synergistic activity of the PARP inhibitor, BMN673, with XPO1 inhibitor, selinexor, in SCLC cells, in mini-PDX models and in SCLC xenograft models. To our knowledge, it is the first time of the preclinical researches combining selinexor and BMN673 in SCLC treatment. The research not only provides promising strategies for the clinical applications but also opens new avenues for the treatment of drug development.

## Author contributions section

Huang Dingzhi: Study design, Funding acquisition, Zhang Yan and Li Lin: Manuscript revision, clinical work on mini-PDX model, Financial support. Yang Guang and Zhiqiang Dong: Novel dual targeting drug design and synthesis. Wang Jingya: Experimental work, Experimental design, Writing, Data analysis. Sun Tao and Jiang Richeng: Experiment design, Paper revision. Qin Tingting: RNA-seq sample preparation. Meng Zhaoting, Zhang Miao, Yu Jiangyong and Bie Zhixin: Clinical work on mini-PDX model. Wang Liuchun, Li Mengjie and Chen Jinliang: Data interpretation. Jiang Xiangli and Lin Li: Software. Zhang Cuicui and Liu Zhujun: In vivo experiments performing.

## Declaration of competing interest

The authors declare that they have no known competing financial interests or personal relationships that could have appeared to influence the work reported in this paper.

## Appendix A. Supplementary data

Supplementary data to this article can be found online at https://doi.org/10.1016/j.canlet.2021.01.008.

## References

[1] R. Govindan, N. Page, D. Morgensztern, W. Read, R. Tierney, A. Vlahiotis, E. L. Spitznagel, J. Piccirillo, Changing epidemiology of small-cell lung cancer in the United States over the last 30 years: analysis of the surveillance, epidemiologic, and end results database, J. Clin. Oncol. 24 (2006) 4539–4544.

[2] J. George, J.S. Lim, S.J. Jang, Y. Cun, L. Ozretic, G. Kong, F. Leenders, X. Lu, L. Fernandez-Cuesta, G. Bosco, C. Muller, I. Dahmen, N.S. Jahchan, K.S. Park, D. Yang, A.N. Karnezis, D. Vaka, A. Torres, M.S. Wang, J.O. Korbel, R. Menon, S. M. Chun, D. Kim, M. Wilkerson, N. Hayes, D. Engelmann, B. Putzer, M. Bos, S. Michels, I. Vlasic, D. Seidel, B. Pinther, P. Schaub, C. Becker, J. Altmuller, J. Yokota, T. Kohno, R. Iwakawa, K. Tsuta, M. Noguchi, T. Muley, H. Hoffmann, P. A. Schnabel, I. Petersen, Y. Chen, A. Soltermann, V. Tischler, C.M. Choi, Y.H. Kim, P.P. Massion, Y. Zou, D. Jovanovic, M. Kontic, G.M. Wright, P.A. Russell, B. Solomon, I. Koch, M. Lindner, L.A. Muscarella, A. la Torre, J.K. Field, M. Jakopovic, J. Knezevic, E. Castanos-Velez, L. Roz, U. Pastorino, O.T. Brustugun, M. Lund-Iversen, E. Thunnissen, J. Kohler, M. Schuler, J. Botling, M. Sandelin, M. Sanchez-Cespedes, H.B. Salvesen, V. Achter, U. Lang, M. Bogus, P.M. Schneider, T. Zander, S. Ansen, M. Hallek, J. Wolf, M. Vingron, Y. Yatabe, W.D. Travis, P. Nurnberg, C. Reinhardt, S. Perner, L. Heukamp, R. Buttner, S.A. Haas, E. Brambilla, M. Peifer, J. Sage, R.K. Thomas, Comprehensive genomic profiles of small cell lung cancer, Nature 524 (2015) 47–53.

[3] A.S. Ireland, A.M. Micinski, D.W. Kastner, B. Guo, S.J. Wait, K.B. Spainhower, C. C. Conley, O.S. Chen, M.R. Guthrie, D. Soltero, Y. Qiao, X. Huang, S. Tarapcsak, S. Devarakonda, M.D. Chalishazar, J. Gertz, J.C. Moser, G. Marth, S. Puri, B.L. Witt, B.T. Spike, T.G. Oliver, MYC drives temporal evolution of small cell lung cancer subtypes by reprogramming neuroendocrine fate, Canc. Cell 38 (2020) 60–78.e12.

[4] A. Augert, H. Mathsyaraja, A.H. Ibrahim, B. Freie, M.J. Geuenich, P.F. Cheng, S. P. Alibeckoff, N. Wu, J.B. Hiatt, R. Basom, A. Gazdar, L.B. Sullivan, R.N. Eisenman, D. MacPherson, MAX functions as a tumor suppressor and rewires metabolism in small cell lung cancer, Canc. Cell 38 (2020) 97–114, e117.

[5] W.S. el-Deiry, T. Tokino, V.E. Velculescu, D.B. Levy, R. Parsons, J.M. Trent, D. Lin, W.E. Mercer, K.W. Kinzler, B. Vogelstein, WAF1, a potential mediator of p53 tumor suppression, Cell 75 (1993) 817–825.

[6] H. Farmer, N. McCabe, C.J. Lord, A.N.J. Tutt, D.A. Johnson, T.B. Richardson, M. Santarosa, K.J. Dillon, I. Hickson, C. Knights, N.M.B. Martin, S.P. Jackson, G.C. M. Smith, A. Ashworth, Targeting the DNA repair defect in BRCA mutant cells as a therapeutic strategy, Nature 434 (2005) 917–921.

[7] N. McCabe, N.C. Turner, C.J. Lord, K. Kluzek, A. Bialkowska, S. Swift, S. Giavara, M.J. O'Connor, A.N. Tutt, M.Z. Zdzienicka, G.C. Smith, A. Ashworth, Deficiency in the repair of DNA damage by homologous recombination and sensitivity to poly (ADP-ribose) polymerase inhibition, Canc. Res. 66 (2006) 8109–8115.

[8] L.A. Byers, J. Wang, M.B. Nilsson, J. Fujimoto, P. Saintigny, J. Yordy, U. Giri, M. Peyton, Y.H. Fan, L.X. Diao, F. Masrorpour, L. Shen, W.B. Liu, B. Duchemann, P. Tumula, V. Bhardwaj, J. Welsh, S. Weber, B.S. Glisson, N. Kalhor, I.I. Wistuba, L. Girard, S.M. Lippman, G.B. Mills, K.R. Coombes, J.N. Weinstein, J.D. Minna, J. V. Heymach, Proteomic profiling identifies dysregulated pathways in small cell lung cancer and novel therapeutic targets including PARP1, Canc. Discov. 2 (2012) 798–811.

[9] A.N. Weaver, E.S. Yang, Beyond DNA repair: additional functions of PARP-1 in cancer, Front. Oncol. 3 (2013) 290.

[10] M. Hussain, J. Mateo, K. Fizazi, F. Saad, N. Shore, S. Sandhu, K.N. Chi, O. Sartor, N. Agarwal, D. Olmos, A. Thiery-Vuillemin, P. Twardowski, G. Roubaud, M. Ozguroglu, J. Kang, J. Burgents, C. Gresty, T. Corcoran, C.A. Adelman, J. de Bono, P.R.T. Investigators, Survival with olaparib in metastatic castration-resistant prostate cancer, N. Engl. J. Med. 383 (2020) 2345–2357.

*J. Wang et al.*                                                      *Cancer Letters 503 (2021) 197–212*

[11] J. de Bono, R.K. Ramanathan, L. Mina, R. Chugh, J. Glaspy, S. Rafii, S. Kaye, J. Sachdev, J. Heymach, D.C. Smith, J.W. Henshaw, A. Herriott, M. Patterson, N.J. Curtin, L.A. Byers, Z.A. Wainberg, Phase I, dose-escalation, two-Part Trial of the PARP inhibitor talazoparib in patients with advanced germline BRCA1/2 mutations and selected sporadic cancers, Canc. Discov. 7 (2017) 620–629.

[12] M.C. Pietanza, S.N. Waqar, L.M. Krug, A. Dowlati, C.L. Hann, A. Chiappori, T.K. Owonikoko, K.M. Woo, R.J. Cardnell, J. Fujimoto, L. Long, L. Diao, J. Wang, Y. Bensman, B. Hurtado, P. de Groot, E.P. Sulman, I.I. Wistuba, A. Chen, M. Fleisher, J.V. Heymach, M.G. Kris, C.M. Rudin, L.A. Byers, Randomized, double-blind, phase II study of temozolomide in combination with either veliparib or placebo in patients with relapsed-sensitive or refractory small-cell lung cancer, J. Clin. Oncol. 36 (2018) 2386–2394.

[13] F. Atrafi, H.J.M. Groen, L.A. Byers, E. Garralda, M.P. Lolkema, R.S. Sangha, S. Viteri, Y.K. Chae, D.R. Camidge, N.Y. Gabrail, B. Hu, T. Tian, S. Nuthalapati, E. Hoening, L. He, P. Komarnitsky, A. Calles, A phase I dose-escalation study of veliparib combined with carboplatin and etoposide in patients with extensive-stage small cell lung cancer and other solid tumors, Clin. Canc. Res. 25 (2019) 496–505.

[14] T.K. Owonikoko, S.E. Dahlberg, G.L. Sica, L.I. Wagner, J.L. Wade 3rd, G. Srkalovic, B.W. Lash, J.W. Leach, T.B. Leal, C. Aggarwal, S.S. Ramalingam, Randomized phase II trial of cisplatin and etoposide in combination with veliparib or placebo for extensive-stage small-cell lung cancer: ECOG-ACRIN 2511 study, J. Clin. Oncol. 37 (2019) 222–229.

[15] R.J. Cardnell, Y. Feng, L. Diao, Y.H. Fan, F. Masrorpour, J. Wang, Y. Shen, G.B. Mills, J.D. Minna, J.V. Heymach, L.A. Byers, Proteomic markers of DNA repair and PI3K pathway activation predict response to the PARP inhibitor BMN 673 in small cell lung cancer, Clin. Canc. Res. 19 (2013) 6322–6328.

[16] R.J. Cardnell, Y. Feng, S. Mukherjee, L. Diao, P. Tong, C.A. Stewart, F. Masrorpour, Y. Fan, M. Nilsson, Y. Shen, J.V. Heymach, J. Wang, L.A. Byers, Activation of the PI3K/mTOR pathway following PARP inhibition in small cell lung cancer, PloS One 11 (2016) e0152584.

[17] K. Balaji, S. Vijayaraghavan, L.X. Diao, P. Tong, Y.H. Fan, J.P.W. Carey, T.N. Bui, S. Warner, J.V. Heymach, K.K. Hunt, J. Wang, L.A. Byers, K. Keyomarsi, AXL inhibition suppresses the DNA damage response and sensitizes cells to PARP inhibition in multiple cancers, Mol. Canc. Res. 15 (2017) 45–58.

[18] A. Lallo, K.K. Frese, C.J. Morrow, R. Sloane, S. Gulati, M.W. Schenk, F. Trapani, N. Simms, M. Galvin, S. Brown, C.L. Hodgkinson, L. Priest, A. Hughes, Z.W. Lai, E. Cadogan, G. Khandelwal, K.L. Simpson, C. Miller, F. Blackhall, M.J. O'Connor, C. Dive, The combination of the PARP inhibitor olaparib and the WEE1 inhibitor AZD1775 as a new therapeutic option for small cell lung cancer, Clin. Canc. Res. 24 (2018) 5153–5164.

[19] P. Chowdhury, P. Dey, S. Ghosh, A. Sarma, U. Ghosh, Reduction of metastatic potential by inhibiting EGFR/Akt/p38/ERK signaling pathway and epithelial-mesenchymal transition after carbon ion exposure is potentiated by PARP-1 inhibition in non-small-cell lung cancer, BMC Canc. 19 (2019) 829.

[20] J.E. Allen, G. Krigsfeld, P.A. Mayes, L. Patel, D.T. Dicker, A.S. Patel, N.G. Dolloff, E. Messaris, K.A. Scata, W. Wang, J.Y. Zhou, G.S. Wu, W.S. El-Deiry, Dual inactivation of Akt and ERK by TIC10 signals Foxo3a nuclear translocation, TRAIL gene induction, and potent antitumor effects, Sci. Transl. Med. 5 (2013) 171ra117.

[21] F. Buontempo, F. Chiarini, D. Bressanin, G. Tabellini, F. Melchionda, A. Pession, M. Fini, L.M. Neri, J.A. McCubrey, A.M. Martelli, Activity of the selective IkappaB kinase inhibitor BMS-345541 against T-cell acute lymphoblastic leukemia: involvement of FOXO3a, Cell Cycle 11 (2012) 2467–2475.

[22] W.B. Tsai, Y.M. Chung, Y. Takahashi, Z.H. Xu, M.C.T. Hu, Functional interaction between FOXO3a and ATM regulates DNA damage response (vol 10, pg 460, 2008), Nat. Cell Biol. 11 (2009), 13871387.

[23] Y.H. Ibrahim, C. Garcia-Garcia, V. Serra, L. He, K. Torres-Lockhart, A. Prat, P. Anton, P. Cozar, M. Guzman, J. Grueso, O. Rodriguez, M.T. Calvo, C. Aura, O. Diez, I.T. Rubio, J. Perez, J. Rodon, J. Cortes, L.W. Ellisen, M. Scaltriti, J. Baselga, PI3K inhibition impairs BRCA1/2 expression and sensitizes BRCA-proficient triple-negative breast cancer to PARP inhibition, Canc. Discov. 2 (2012) 1036–1047.

[24] M.C. Hu, D.F. Lee, W. Xia, L.S. Golfman, F. Ou-Yang, J.Y. Yang, Y. Zou, S. Bao, N. Hanada, H. Saso, R. Kobayashi, M.C. Hung, IkappaB kinase promotes tumorigenesis through inhibition of forkhead FOXO3a, Cell 117 (2004) 225–237.

[25] N. Chapuis, S. Park, L. Leotoing, J. Tamburini, F. Verdier, V. Bardet, A.S. Green, L. Willems, F. Agou, N. Ifrah, F. Dreyfus, G. Bismuth, V. Baud, C. Lacombe, P. Mayeux, D. Bouscary, IkappaB kinase overcomes PI3K/Akt and ERK/MAPK to control FOXO3a activity in acute myeloid leukemia, Blood 116 (2010) 4240–4250.

[26] S.K. Roy, R.K. Srivastava, S. Shankar, Inhibition of PI3K/AKT and MAPK/ERK pathways causes activation of FOXO transcription factor, leading to cell cycle arrest and apoptosis in pancreatic cancer, J. Mol. Signal. 5 (2010) 10.

[27] Y. Perez-Riverol, A. Csordas, J. Bai, M. Bernal-Llinares, S. Hewapathirana, D.J. Kundu, A. Inuganti, J. Griss, G. Mayer, M. Eisenacher, E. Perez, J. Uszkoreit, J. Pfeuffer, T. Sachsenberg, S. Yilmaz, S. Tiwary, J. Cox, E. Audain, M. Walzer, A.F. Jarnuczak, T. Ternent, A. Brazma, J.A. Vizcaino, The PRIDE database and related tools and resources in 2019: improving support for quantification data, Nucleic Acids Res. 47 (2019) D442–D450.

[28] F. Zhang, W. Wang, Y. Long, H. Liu, J. Cheng, L. Guo, R. Li, C. Meng, S. Yu, Q. Zhao, S. Lu, L. Wang, H. Wang, D. Wen, Characterization of drug responses of mini patient-derived xenografts in mice for predicting cancer patient clinical therapeutic response, Canc. Commun. 38 (2018) 60.

[29] P. Zhao, H. Chen, D. Wen, S. Mou, F. Zhang, S. Zheng, Personalized treatment based on mini patient-derived xenografts and WES/RNA sequencing in a patient with metastatic duodenal adenocarcinoma, Canc. Commun. 38 (2018) 54.

[30] M. Ghandi, F.W. Huang, J. Jane-Valbuena, G.V. Kryukov, C.C. Lo, E.R. McDonald 3rd, J. Barretina, E.T. Gelfand, C.M. Bielski, H. Li, K. Hu, A.

Y. Andreev-Drakhlin, J. Kim, J.M. Hess, B.J. Haas, F. Aguet, B.A. Weir, M.V. Rothberg, B.R. Paolella, M.S. Lawrence, R. Akbani, Y. Lu, H.L. Tiv, P.C. Gokhale, A. de Weck, A.A. Mansour, C. Oh, J. Shih, K. Hadi, Y. Rosen, J. Bistline, K. Venkatesan, A. Reddy, D. Sonkin, M. Liu, J. Lehar, J.M. Korn, D.A. Porter, M.D. Jones, J. Golji, G. Caponigro, J.E. Taylor, C.M. Dunning, A.L. Creech, A.C. Warren, J.M. McFarland, M. Zamanighomi, A. Kauffmann, N. Stransky, M. Imielinski, Y.E. Maruvka, A.D. Cherniack, A. Tsherniak, F. Vazquez, J.D. Jaffe, A.A. Lane, D.M. Weinstock, C.M. Johannessen, M.P. Morrissey, F. Stegmeier, R. Schlegel, W.C. Hahn, G. Getz, G.B. Mills, J.S. Boehm, T.R. Golub, L.A. Garraway, W.R. Sellers, Next-generation characterization of the cancer cell line Encyclopedia, Nature 569 (2019) 503–508.

[31] X. Dong, A. Biswas, K.E. Suel, L.K. Jackson, R. Martinez, H. Gu, Y.M. Chook, Structural basis for leucine-rich nuclear export signal recognition by CRM1, Nature 458 (2009) 1136–1141.

[32] F. Conforti, Y. Wang, J.A. Rodriguez, A.T. Alberobello, Y.W. Zhang, G. Giaccone, Molecular pathways: anticancer activity by inhibition of nucleocytoplasmic shuttling, Clin. Canc. Res. 21 (2015) 4508–4513.

[33] F. Conforti, X. Zhang, G. Rao, T. De Pas, Y. Yonemori, J.A. Rodriguez, J.N. McCutcheon, R. Rahhal, A.T. Alberobello, Y. Wang, Y.W. Zhang, G. Guha, G. Giaccone, Therapeutic effects of XPO1 inhibition in thymic epithelial tumors, Canc. Res. 77 (2017) 5614–5627.

[34] H. You, K. Yamamoto, T.W. Mak, Regulation of transactivation-independent proapoptotic activity of p53 by FOXO3a, Proc. Natl. Acad. Sci. U. S. A. 103 (2006) 9051–9056.

[35] X.W. Guan, H.Q. Wang, W.W. Ban, Z. Chang, H.Z. Chen, L. Jia, F.T. Liu, Novel HDAC inhibitor Chidamide synergizes with Rituximab to inhibit diffuse large B-cell lymphoma tumour growth by upregulating CD20, Cell Death Dis. 11 (2020) 20.

[36] K. Yuan, Y. Sun, T. Zhou, J. McDonald, Y. Chen, PARP-1 regulates resistance of pancreatic cancer to TRAIL therapy, Clin. Canc. Res. 19 (2013) 4750–4759.

[37] T. Yamada, J.M. Amann, A. Tanimoto, H. Taniguchi, T. Shukuya, C. Timmers, S. Yano, K. Shilo, D.P. Carbone, Histone deacetylase inhibition enhances the antitumor activity of a MEK inhibitor in lung cancer cells harboring RAS mutations, Mol. Canc. Therapeut. 17 (2018) 17–25.

[38] D. Yue, X. Sun, Idelalisib promotes Bim-dependent apoptosis through AKT/FoxO3a in hepatocellular carcinoma, Cell Death Dis. 9 (2018) 935.

[39] J.S. Fridman, S.W. Lowe, Control of apoptosis by p53, Oncogene 22 (2003) 9030–9040.

[40] M. Monsalve, Y. Olmos, The complex biology of FOXO, Curr. Drug Targets 12 (2011) 1322–1350.

[41] P. Ranganathan, T. Kashyap, X. Yu, X. Meng, T.H. Lai, B. McNeil, B. Bhatnagar, S. Shacham, M. Kauffman, A.M. Dorrance, W. Blum, D. Sampath, Y. Landesman, R. Garzon, XPO1 inhibition using selinexor synergizes with chemotherapy in acute myeloid leukemia by targeting DNA repair and restoring topoisomerase IIalpha to the nucleus, Clin. Canc. Res. 22 (2016) 6142–6152.

[42] J.G. Turner, J.L. Dawson, S. Grant, K.H. Shain, W.S. Dalton, Y. Dai, M. Meads, R. Baz, M. Kauffman, S. Shacham, D.M. Sullivan, Treatment of acquired drug resistance in multiple myeloma by combination therapy with XPO1 and topoisomerase II inhibitors, J. Hematol. Oncol. 9 (2016) 73.

[43] P. Karran, DNA double strand break repair in mammalian cells, Curr. Opin. Genet. Dev. 10 (2000) 144–150.

[44] C.S. Sorensen, L.T. Hansen, J. Dziegielewski, R.G. Syljuasen, C. Lundin, J. Bartek, T. Helleday, The cell-cycle checkpoint kinase Chk1 is required for mammalian homologous recombination repair, Nat. Cell Biol. 7 (2005) 195–201.

[45] P. Baumann, F.E. Benson, S.C. West, Human Rad51 protein promotes ATP-dependent homologous pairing and strand transfer reactions in vitro, Cell 87 (1996) 757–766.

[46] P. Baumann, S.C. West, Role of the human RAD51 protein in homologous recombination and double-stranded-break repair, Trends Biochem. Sci. 23 (1998) 247–251.

[47] F.E. Benson, P. Baumann, S.C. West, Synergistic actions of Rad51 and Rad52 in recombination and DNA repair, Nature 391 (1998) 401–404.

[48] G. Poulogiannis, I.M. Frayling, M.J. Arends, DNA mismatch repair deficiency in sporadic colorectal cancer and Lynch syndrome, Histopathology 56 (2010) 167–179.

[49] H.E. Bryant, N. Schultz, H.D. Thomas, K.M. Parker, D. Flower, E. Lopez, S. Kyle, M. Meuth, N.J. Curtin, T. Helleday, Specific killing of BRCA2-deficient tumours with inhibitors of poly(ADP-ribose) polymerase, Nature 434 (2005) 913–917.

[50] A. Drean, C.J. Lord, A. Ashworth, PARP inhibitor combination therapy, Crit. Rev. Oncol. Hematol. 108 (2016) 73–85.

[51] K.D. Courtney, R.B. Corcoran, J.A. Engelman, The PI3K pathway as drug target in human cancer, J. Clin. Oncol. 28 (2010) 1075–1083.

[52] U. Banerji, E.J. Dean, J.A. Perez-Fidalgo, G. Batist, P.L. Bedard, B. You, S.N. Westin, P. Kabos, M.D. Garrett, M. Tall, H. Ambrose, J.C. Barrett, T.H. Carr, S.Y.A. Cheung, C. Corcoran, M. Cullberg, B.R. Davies, E.C. de Bruin, P. Elvin, A. Foxley, P. Lawrence, J.P.O. Lindemann, R. Maudsley, M. Pass, V. Rowlands, P. Rugman, G. Schiavon, J. Yates, J.H.M. Schellens, A phase I open-label study to identify a dosing regimen of the pan-AKT inhibitor AZD5363 for evaluation in solid tumors and in PIK3CA-mutated breast and gynecologic cancers, Clin. Canc. Res. 24 (2018) 2050–2059.

[53] S. Matkar, C. An, X. Hua, Kinase inhibitors of HER2/AKT pathway induce ERK phosphorylation via a FOXO-dependent feedback loop, Am. J. Canc. Res. 7 (2017) 1476–1485.

[54] K. Lin, H. Hsin, N. Libina, C. Kenyon, Regulation of the Caenorhabditis elegans longevity protein DAF-16 by insulin/IGF-1 and germline signaling, Nat. Genet. 28 (2001) 139–145.

211

[55] D.S. Hwangbo, B. Gershman, M.P. Tu, M. Palmer, M. Tatar, Drosophila dFOXO controls lifespan and regulates insulin signalling in brain and fat body, Nature 429 (2004) 562–566.

[56] J. Gilley, P.J. Coffer, J. Ham, FOXO transcription factors directly activate bim gene expression and promote apoptosis in sympathetic neurons, J. Cell Biol. 162 (2003) 613–622.

[57] K.T. Nguyen, M.P. Holloway, R.A. Altura, The CRM1 nuclear export protein in normal development and disease, Int. J. Biochem. Mol. Biol. 3 (2012) 137–151.

[58] D. Xu, N.V. Grishin, Y.M. Chook, NESdb: a database of NES-containing CRM1 cargoes, Mol. Biol. Cell 23 (2012) 3673–3676.

[59] N. Saenz-Ponce, R. Pillay, L.M. de Long, T. Kashyap, C. Argueta, Y. Landesman, M. Hazar-Rethinam, S. Boros, B. Panizza, M. Jacquemyn, D. Daelemans, O. M. Gannon, N.A. Saunders, Targeting the XPO1-dependent nuclear export of E2F7 reverses anthracycline resistance in head and neck squamous cell carcinomas, Sci. Transl. Med. 10 (2018).

[60] U. Kutay, M.W. Hetzer, Reorganization of the nuclear envelope during open mitosis, Curr. Opin. Cell Biol. 20 (2008) 669–677.

[61] J.G. Turner, D.M. Sullivan, CRM1-mediated nuclear export of proteins and drug resistance in cancer, Curr. Med. Chem. 15 (2008) 2648–2655.

[62] J.G. Turner, J. Dawson, D.M. Sullivan, Nuclear export of proteins and drug resistance in cancer, Biochem. Pharmacol. 83 (2012) 1021–1032.

[63] C.J. Lord, A. Ashworth, PARP inhibitors: synthetic lethality in the clinic, Science 355 (2017) 1152–1158.

[64] S. Xu, M. Zhan, C. Jiang, M. He, L. Yang, H. Shen, S. Huang, X. Huang, R. Lin, Y. Shi, Q. Liu, W. Chen, M. Mohan, J. Wang, Genome-wide CRISPR screen identifies ELP5 as a determinant of gemcitabine sensitivity in gallbladder cancer, Nat. Commun. 10 (2019) 5492.

[65] H. You, T.W. Mak, Crosstalk between p53 and FOXO transcription factors, Cell Cycle 4 (2005) 37–38.